*Journal of Statistical Physics, Vol. 108, Nos. 3/4, August 2002 (© 2002)*

# The Ising Partition Function for 2D Grids with Periodic Boundary: Computation and Analysis

**Roland Häggkvist**[1] **and Per Håkan Lundow**[2]

*Received November 30, 2001; accepted March 11, 2002*

The Ising partition function for a graph counts the number of bipartitions of the vertices with given sizes, with a given size of the induced edge cut. Expressed as a 2-variable generating function it is easily translatable into the corresponding partition function studied in statistical physics. In the current paper a comparatively efficient transfer matrix method is described for computing the generating function for the $n \times n$ grid with periodic boundary. We have applied the method to up to the $15 \times 15$ grid, in total 225 vertices. We examine the phase transition that takes place when the edge cut reaches a certain critical size. From the physical partition function we extract quantities such as magnetisation and susceptibility and study their asymptotic behaviour at the critical temperature.

**KEY WORDS:** 2D Ising model; partition function; external non-zero field; exact computation; transfer matrix.

## 1. INTRODUCTION

The Ising model of ferromagnetism has been thoroughly studied since its conception in the 1920's. It was solved in the 1-dimensional case by Ernst Ising himself and in the (infinite) 2-dimensional case without an external field by Lars Onsager in 1944. Somewhat later Bruria Kaufman gave a zero field solution for the finite rectangular grid, with or without cyclic boundaries. For an introduction see ref. 1. The model is centered around a partition function which in the general case is notoriously hard to compute although it is easy to formulate. The Ising partition function, formal definition below, can be computed in polynomial time for graphs imbedded in

[1] Department of Mathematics, Umeå University, SE-901 87 Umeå, Sweden; e-mail: roland.haggkvist@math.umu.se

[2] Condensed Matter Theory, Department of Physics, Royal Institute of Technology, SE-106 91 Stockholm, Sweden; e-mail: phl@theophys.kth.se



0022-4715/02/0800-0429/0 © 2002 Plenum Publishing Corporation

surfaces of low genus when the external field is excluded. In particular, Beale[2] has made an easy-to-use program in Mathematica which implements Kaufmans solution for the zero field partition function for the $m \times n$ grid with periodic boundary. Using this program, a desktop computer easily computes the partition function for, say, the $64 \times 64$ grid in a few days.

The situation becomes very different when we add the external field. If we stay with oblong objects, the easiest to handle are graphs of the form $G \times P_n$ where $G$ is a graph, hopefully with many automorphisms, and $P_n$ denotes the path with $n$ vertices. Thus $P_m \times P_n$ denotes the $m \times n$ grid with open boundary, $C_m \times P_n$ the $m \times n$ grid which is periodic in the first direction and open in the second (we refer to this as a semiopen $m \times n$ grid), while $C_m \times C_n$ denotes the closed $m \times n$ grid. Of these three families the easiest by far to handle seems to be the semiopen kind.

In ref. 3 it is described how to use the dihedral group in order to simplify the computation of, for instance, the Ising partition function for the graph $C_m \times P_n$ and this computation has been performed for $m \cdot n \leqslant 220$ when $m \leqslant 11$ and also for $m = n \leqslant 13$. In ref. 4 the full partition function (i.e., with external field) is computed for a number of grids with open boundary. The largest square shaped of these was the $16 \times 16$ grid with open boundary. We have computed a complete set of partition functions for $P_m \times P_n$ where $m + n \leqslant 27$ and also for $m \cdot n \leqslant 180$.

The current article reports an improved method for computing the full partition function for $n \times n$ grids with periodic boundary. We have applied it successfully to the case $n \leqslant 15$. Previously, the largest square shaped grid with periodic boundary to be studied was the $10 \times 10$ grid by Baker.[5] He divided the graph into smaller manageable parts, and, using the inherent Markov property of the Ising partition function, managed to compute numerically several quantities of physical interest at some thirty temperature points in double precision. However, although Baker makes use of an exactly computed intermediate polynomimal from which it in principle is possible to obtain the exact Ising partition function by (time consuming) change of variables he does not in fact obtain the coefficients of the partition function (neither exactly nor in double precision). We, in contrast, do.

The method described here is based on the use of transfer matrices. The curse of this method is that it involves the computation of the traces of very large matrices, which tend to have entries that are formal polynomials in two variables. The traditional method, see, e.g., ref. 6, involves the computation of the trace of the $n$th power of a square matrix of order $2^n$. This method can today be used for the $10 \times 10$ grid, say, but then it requires gigabytes of memory and some skillful programming. We have performed this particular computation using a 2 gigabyte node for a week

in 1998 at the Center for Parallel Computers in Stockholm. The source code, written in Fortran 90, and the resulting polynomials can be downloaded from http://www.math.umu.se/~phl.

The method described in the current paper is also exponential, but substantially faster and less space consuming. It involves computing the trace of the product of $2n$ matrices each of order at most $2^{\lfloor n/2 \rfloor}$. This method made it possible to run the $10 \times 10$ case on a Macintosh 9600 computer in 5.5 hours (yes, the two runs gave the same output).

A periodic boundary is beneficial from a theoretical point of view since it makes the graph regular, and indeed, vertex transitive. This adds substantial symmetry, which in principle can be used to reduce the amount of necessary work.

What we actually compute is a generating function

$$Z(G; x, y) = \sum_{i,j} a_{i,j} x^i y^j$$

for a graph $G$ on $n$ vertices and $m$ edges. Here $a_{i,j}$ is the number of bipartitions of the vertices into sets of order $(n-j)/2$ and $(n+j)/2$ respectively, with $(m-i)/2$ edges between them.

Evaluating the partition function in a certain point gives the partition function typically studied in statistical physics,

$$Z(G; e^{\beta J}, e^{\beta h})$$

where $\beta = -1/kT$. From this partition function we obtain various quantities such as the internal energy, magnetisation, susceptibility etc., these are defined in Section 5. In Section 6 we plot some of these functions and also try to estimate their asymptotic behaviour at the critical temperature in terms of $n$. We also take a quick look at the behaviour on the anti-ferromagnetic side. The partition function $Z(G; x, y)$ itself (i.e., its coefficients) undergoes a phase transition when the edge cut $i$ reaches a certain critical size. At this point the distribution of the difference $j$ in size of the bipartitions goes from unimodal to essentially bimodal. A study of this is made in Section 7.

## 2. NOTATION AND DEFINITIONS

A simple graph $G = (V, E)$ is an ordered pair where $V$ is a set of vertices and $E$, the edges, is a set of 2-subsets of $V$. If $W$ is a subset of $V(G)$ then $G[W]$ is the subgraph of $G$ induced by $W \cdot G - W$ is the graph obtained by deleting the vertices in $W$, i.e., $G[\bar{W}]$, where $\bar{W} = V(G) \setminus W$. If $W_1, W_2 \subseteq V(G)$ then $[W_1, W_2]$ is the set of edges having one end in $W_1$ and

the other in $W_2$. If $F \subseteq E(G)$ then $G-F$ is the graph obtained by deleting the edges $F$ from $G$. Also, $H=(V, F)$ is called a spanning subgraph of $G$. If $F$ is a set of edges having one end in the graph $G$ then $G \cup F$ is the graph $G$ together with the edges $F$ and the vertices at the other end of $F$. We let $P_n$ and $C_n$ denote the path and cycle respectively on $n$ vertices. If $G$ and $H$ are graphs then $G \times H$ denotes the cartesian product of $G$ and $H$. The vertices of $G \times H$ are $\{(v, w): v \in V(G), w \in V(H)\}$. Two vertices $(v_1, w_1)$ and $(v_2, w_2)$ are adjacent iff $v_1 = v_2$ and $\{w_1, w_2\} \in V(H)$ or $w_1 = w_2$ and $\{v_1, v_2\} \in V(G)$. For example, $P_m \times P_n$ is the $m \times n$ grid with open boundary, and $C_m \times C_n$ is the same but with periodic boundary. The function $\sigma: V \to \{-1, +1\}$ is the state of the graph (or, a spin configuration) and $\sigma_v$ is the spin of vertex $v$. The restriction of $\sigma$ to $W$ is denoted $\sigma W$.

**Definition 2.1.** Given a state $\sigma$ we define the energy $v_\sigma(G)$ and magnetisation $\mu_\sigma(G)$ of a graph $G$ as

$$v_\sigma(G) = \sum_{\{u, v\} \in E(G)} \sigma_u \sigma_v \qquad \text{and} \qquad \mu_\sigma(G) = \sum_{v \in V(G)} \sigma_v$$

If $W \subseteq V(G)$ and $F \subseteq E(G)$ then

$$v_\sigma(G, W) = \sum_{\{u, v\} \in [W, W]} \sigma_u \sigma_v,$$

$$v_\sigma(G, F) = \sum_{\{u, v\} \in F} \sigma_u \sigma_v,$$

$$\mu_\sigma(G, W) = \sum_{v \in W} \sigma_v$$

We suppress the $G$ and $\sigma$ from $v$ and $\mu$ when the context leaves no room for ambiguity.

**Definition 2.2.** The Ising partition function $Z(G; x, y)$ for a graph $G=(V, E)$ in variables $x$ and $y$ is defined as

$$Z(G; x, y) = \sum_{\sigma \in \{-1, +1\}^V} x^{v_\sigma(G)} y^{\mu_\sigma(G)}$$

**Definition 2.3.** The coefficients $a_{i,j}$ and $a_i$ is defined by

$$Z(G; x, y) = \sum_{i, j} a_{i, j} x^i y^j \qquad \text{and} \qquad Z(G; x, 1) = \sum_i a_i x^i$$

Since we will use only the variables $x$ and $y$ we henceforth write $Z(G)$. By definition $a_{i,j}$ is the number of states at energy $i$ and magnetisation $j$, and $a_i$ is the number of states at energy $i$. Note that $a_{i,j} = a_{i,-j}$; given a state $\sigma$ we flip each spin to obtain $-\sigma$ and this preserves the energy but reverses the magnetisation. Also, for bipartite graphs we have $a_i = a_{-i}$; flip each spin of one part and the energy of each edge changes its sign. In general though, we have $a_i \neq a_{-i}$.

Let $Z(G, \sigma W)$ be the partition function when the vertices in $W$ keeps their spins fixed to $\sigma W$,

$$Z(G, \sigma W) = \sum_{\sigma \bar{W}} x^{\nu_\sigma(G)} y^{\mu_\sigma(G)}$$

where $\bar{W}$ is the complement of $W$.

## 3. POLYGRAPHS AND TRANSFER MATRICES

We begin this section by introducing the polygraph, as described in ref. 7, see also ref. 6 where they are called graph schemes. A polygraph consists of a set of disjoint graphs $G_1,\ldots, G_p$ and a set of binary relations $X_1,\ldots, X_p$ where $X_i \subseteq V(G_{i-1}) \times V(G_i)$, for $i = 1,\ldots, p$, and the binary relations will be thought of as sets of edges. We count the indices modulo $p$ so that, e.g., $G_0$ means $G_p$ and $G_{p+1}$ means $G_1$. Let $\Omega_p = \Omega(\{G_i\}, \{X_i\}, i = 1,\ldots, p)$ denote the polygraph having vertices $V(G_1) \cup \cdots \cup V(G_p)$ and edges $X_1 \cup E(G_1) \cup \cdots \cup X_p \cup E(G_p)$. A particularly nice polygraph is obtained when $G_i = G$ and $X_i = X$ for $i = 1,\ldots, p$; denote this polygraph by $\Omega(G, X, p)$. For example, if $G = (\{v\}, \varnothing)$ and $X = \{(v, v)\}$, then $\Omega(G, X, p)$ is the cycle on $p$ vertices. Let $D_i$ be the domain of $X_i$ and let $H_i$ be the graph $X_i \cup G_i$ on vertices $D_i \cup V(G_i)$ and edges $X_i \cup E(G_i)$, see Fig. 1. We refer to $D_i$ and $D_{i+1}$ as the in-vertices and out-vertices respectively of $H_i$. Note by the way that $D_i$ and $D_{i+1}$ are disjoint sets.

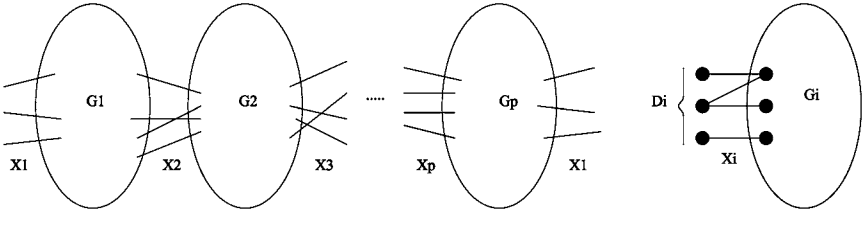


Fig. 1. Structure of polygraph $\Omega_p$ and $H_i$, respectively.

Define the matrices $\mathbf{T}_i$ for $i = 1,\ldots, p$ with entries,

$$\mathbf{T}_i(\zeta, \xi) = Z(H_i, \sigma D_i = \zeta, \sigma D_{i+1} = \xi)\ y^{-\mu(D_i)} \tag{1}$$

The shape of matrix $\mathbf{T}_i$ is $2^{|D_i|} \times 2^{|D_{i+1}|}$. The following theorem holds,

**Theorem 3.1.**

$$\text{trace}(\mathbf{T}_1 \cdots \mathbf{T}_p) = Z(\Omega_p)$$

*Proof.* See, e.g., refs. 4 or 6. ▮

**Example 3.2.** We describe the standard, but inefficient, way of computing $Z(C_n \times C_n)$, this is also found in ref. 6. In the polygraph, let $G$ be the cycle $C_n$ and set $X = \{(i, i) : i = 1,\ldots, n\}$. Then $\Omega_n$ is isomorphic to $C_n \times C_n$. The transfer matrix $\mathbf{T}$ in Eq. (1) then has shape $2^n \times 2^n$ and we need to compute trace($\mathbf{T}^n$), a rather awesome task. Still, it is quite manageable for $n \leqslant 10$ on todays computers.

### 3.1. The Method

We now describe a better way to compute $Z(C_n \times C_n)$. Let $n$ be given. Define $H = P_{n+1}$ as the path on vertices $\{1, 2,\ldots, n+1\}$ with edges $\{\{1, 2\},\ldots, \{n, n+1\}\}$. Define the in-set $I = \{k: 3 \leqslant k \leqslant n, k \text{ odd}\}$, the out-set $J = \{k: 2 \leqslant k \leqslant n, k \text{ even}\}$ and a boundary-set $K = \{1, n+1\}$ so that $I$, $J$ and $K$ are disjoint and $I \cup J \cup K = \{1,\ldots, n+1\}$, see Fig. 2. Define two types of transfer matrices $\mathbf{S}$ and $\mathbf{T}$, four of each,

$$\mathbf{S}_\eta(\zeta, \xi) = Z(H, \sigma I = \zeta, \sigma J = \xi, \sigma K = \eta)\ y^{-\mu(I \cup K)}$$
$$\mathbf{T}_\eta(\zeta, \xi) = Z(H, \sigma J = \zeta, \sigma I = \xi, \sigma K = \eta)\ y^{-\mu(J \cup K)}$$

Note that these matrices have shape $2^{\lfloor \frac{n-1}{2} \rfloor} \times 2^{\lfloor \frac{n}{2} \rfloor}$ and $2^{\lfloor \frac{n}{2} \rfloor} \times 2^{\lfloor \frac{n-1}{2} \rfloor}$ respectively, considerably smaller than the matrix in Example 3.2. Step by step we will now build up our grid, each matrix product corresponding to the addition of a path on the diagonal of the grid.

**Theorem 3.3.** Let $K_i$ be the boundary-set at the $i$th step. Then

$$\text{trace}(S_{\eta_1} T_{\eta_2} \cdots S_{\eta_{p-1}} T_{\eta_p}) = Z(\Omega_p, \sigma K_1 = \eta_1,\ldots, \sigma K_p = \eta_p)\ y^{-\mu(K_1 \cup \cdots \cup K_p)}$$

*Proof.* The result follows from Theorem 3.1. ▮

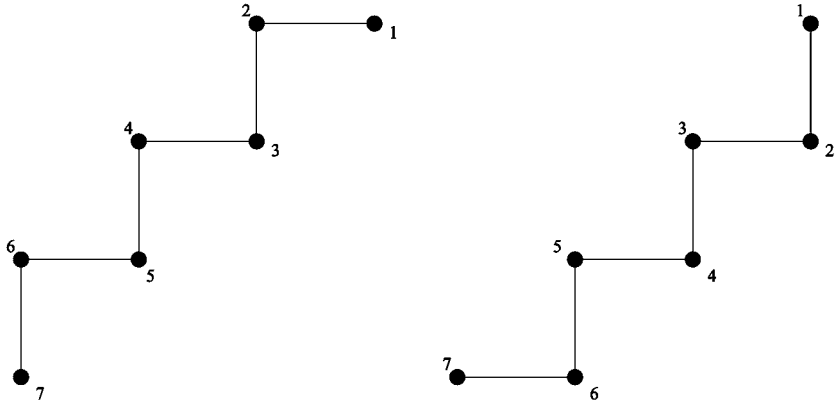


Fig. 2. $P_7$ at odd steps (left) and even steps (right).

Now consider Figs. 3 and 4 where each step is a path with edges marked as dashed lines or full lines. If we identify the vertices labelled with the same number then the polygraph $\Omega_{2n}$ is isomorphic to the graph $C_n \times C_n$. With the right choice of spins $\eta_i$ on the boundary-sets the last theorem gives us the desired partition function. Before we continue some notation is needed. Let $\eta_{i,j}$ denote the spin of vertex $j$ in graph $H$ at step $i$

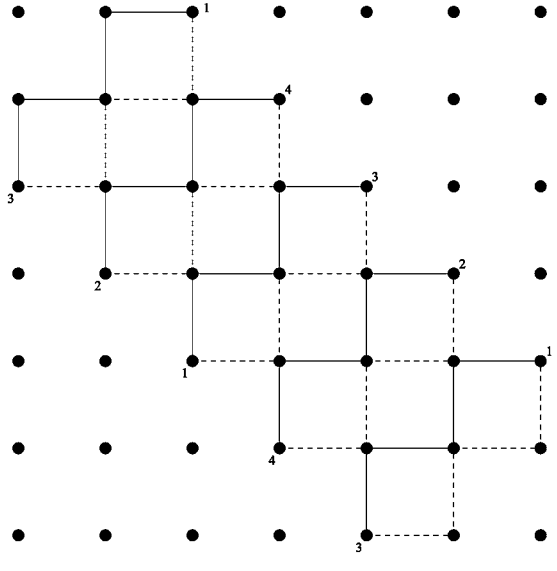


Fig. 3. The even case, $n = 4$.

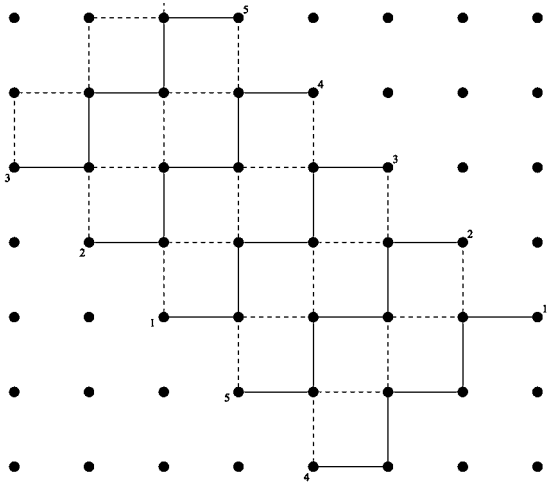


Fig. 4. The odd case, $n = 5$.

so that $\sigma K_i = \eta_i = (\eta_{i,1}, \eta_{i,n+1})$. We count the step index $i$ modulo $2n$ so that, e.g., $K_0$ and $K_{2n+1}$ are identical to $K_{2n}$ and $K_1$ respectively. Given a boundary $\eta_{1,1}, \eta_{2,1},\ldots, \eta_{2n,1}$ it must fulfill that $\eta_{2i,1} = \eta_{2i+1,1}$ and $\eta_{2i,1} = \eta_{2i+n,n+1}$ for $i = 1,\ldots, n$ since these pairs refer to the same vertices. If $n$ is even we must also have that $\eta_{2i,n+1} = \eta_{2i+1,n+1}$ and if $n$ is odd then we must have $\eta_{2i,n+1} = \eta_{2i-1,n+1}$ since these pairs again refer to the same vertices. With these restrictions we only have to specify the $\eta_{2,1}, \eta_{4,1},\ldots, \eta_{2n,1}$ (or the odd steps if that is preferred) since this also defines the remaining $\eta_{i,j}$. Let $L$ be this set of $n$ vertices on the diagonal, see Figs. 3 and 4. Then by choosing a spin-configuration $\sigma L$ we have also chosen a spin-configuration $\eta = (\eta_1,\ldots, \eta_{2n})$ of $K_1,\ldots, K_{2n}$ by using our rules above. If we use Theorem 3.3 we thus obtain,

**Theorem 3.4.**

$$Z(C_n \times C_n) = \sum_{\sigma L} Z(C_n \times C_n, \sigma L)$$
$$= \sum_{\sigma L} \operatorname{trace}(\mathbf{S}_{\eta_1} \mathbf{T}_{\eta_2} \cdots \mathbf{S}_{\eta_{2n-1}} \mathbf{T}_{\eta_{2n}})\, y^{\mu(L)}$$

## 3.2. Symmetry and Tricks

In Theorem 3.4 the sum contains $2^n$ terms, each term corresponding to a state of the boundary set $L$. We can however cut down on the amount of summation work by approximately a factor $4n$. The obvious reduction in work

is to only take the sum over all non-isomorphic states. Note that $L$ has the automorphism group of a cycle on $n$ vertices, i.e., it has $2n$ automorphisms. This reduces the number of terms by approximately a factor $2n$.

The second trick is to note that if $\sigma$ is a state of $G$ with energy $i$ and magnetisation $j$ then the complementary state $-\sigma$ (obtained by setting each $\sigma_v$ to its negative value) has the same energy but magnetisation $-j$. To compute a partition function $Z$ from Definition 2.2 we then have to take the sum over only half of the states, such as those states where one vertex has its spin fixed to $+1$, and obtain the sum over the complementary states afterwards.

Another way to use this is to compute a partial partition function, such as the sum over the states with negative magnetisation. Let $P = \sum a_{i,j} x^i y^j$ be this sum. To obtain the sum over the states with positive magnetisation we compute the complementary partition function $\bar{P} = \sum a_{i,j} x^i y^{-j}$. The states with magnetisation exactly 0 would have to be treated separately though.

Now, let $U \subseteq V(G)$ for some graph $G$ where $u = |U|$. We define two partial polynomials for when at most $u/2$ vertices in $U$ have been set to spin $+1$; one for $\mu(U) < 0$ and one for $\mu(U) = 0$,

$$Z^*(G) = \sum_{\substack{\sigma U \\ \mu(U) < 0}} Z(G; \sigma U)$$

$$Z^{**}(G) = \sum_{\substack{\sigma U \\ \mu(U) = 0}} Z(G; \sigma U)$$

With these definitions we have

$$Z(G) = Z^*(G) + \bar{Z}^*(G) + Z^{**}(G)$$

Note that $Z^{**}(G) = 0$ when $u$ is odd.

We apply this formula to our circumstances by setting $U$ to the boundary $L$ in Theorem 3.4 and letting $G = C_n \times C_n$. Let $\{\theta_1, \ldots, \theta_s\}$ be the set of non-isomorphic states $\sigma L$ having weights $w_1, \ldots, w_s$, i.e., $\theta_k$ represents $w_k$ different states, such that $\mu(L) \leqslant 0$. Also, let the $r$ first of the $\theta_k$'s have $\mu(L) < 0$. With the following formulae we conclude our description of the computational process,

$$\begin{aligned} Z^*(G) &= \sum_{k=1}^{r} w_k Z(G; \sigma L = \theta_k) \\ Z^{**}(G) &= \sum_{k=r+1}^{s} w_k Z(G; \sigma L = \theta_k) \\ Z(G) &= Z^*(G) + \bar{Z}^*(G) + Z^{**}(G) \end{aligned} \tag{2}$$

## 4. PRACTICAL CONSIDERATIONS

The algorithm implicit in the previous sections was implemented in Fortran 90 and run in parallel using both MPI (for communication between nodes) and OpenMP on a set of 8-way Nighthawk shared-memory nodes at the Center for Parallel Computers in Stockholm. The problem is very suited to running on a parallel computer, being embarrasingly parallel by its nature. In total, the computation for the $15 \times 15$ grid took a little more than 7 node-months, about 5 cpu-years since each node has 8 cpu's. Unfortunately though, the total running time increases more than a factor 8 each time the grids linear size is increased by 1. Memory requirements were not very imposing, only a few hundred megabytes for $n = 15$, though this will increase rapidly for each larger grid, more on this below.

Central parts of the software are a module for multi precision integers,[8] and a module for polynomials,[9] adapted for shared-memory nodes. The entries of the transfer matrices, which only contains monomials with coefficient one, can be computed very fast with a few bit-operations and are returned by functions. It is then unnecessary to store the entire matrix, we only need to store vectors containing polynomials. The data files containing the resulting polynomials and the complete set of source code can be obtained from one of the authors (P.H. Lundow), or you can download it from `http://www.math.umu.se/~phl`.

We will give a brief description of what seems to be a good way to organise the computations in practice and at the same time summarise the previous section. First of all we need to determine the set of non-isomorphic spin-configurations $\sigma L$, i.e., the set $\{\theta_1,\ldots,\theta_s\}$ and their corresponding weights $w_1,\ldots,w_s$. In other terms we obtain the set of non-isomorphic 2-colourings (using colours $\pm 1$) of the vertices in the cycle $C_n$, though we keep only those with at most $n/2$ vertices coloured 1. Store all of these in a file and pick out the $k$th colouring which will then be designated the $k$th case. There will be somewhat more than $2^{n-2}/n$ cases to run through.

Now we compute the partition functions $Z(G; \sigma L = \theta_k)$. Given a $\theta_k$, which is a spin-configuration of $n$ vertices, we can determine the set of boundaries $\eta_i$ of Theorem 3.3 for $i = 1,\ldots,2n$. Having done that we need to generate the matrices $\mathbf{S}_\eta$ and $\mathbf{T}_\eta$. Each position, which contains a monomial in two variables, is easily generated with a few bit-operations.

What is left is to compute the trace of a matrix product. Of course, one doesn't have to compute the entire matrix product but only the diagonal elements of the product and this is done by taking vector-matrix products. At this point we distribute the computations onto individual nodes and let each node compute its fair share of the $2^{\lfloor \frac{n-1}{2} \rfloor}$ diagonal elements. Note by the way that for even $n$ the matrices have different shapes.

If we now have multi-processor nodes with shared memory (a parallell architecture which is gaining ground) an efficient level of exploiting this is to distribute the vector-matrix product onto the individual processors. That is, each processor computes its fair share of the elements in the vector that results from each vector-matrix product. This gave an almost 100 percent usage of each node. This is the point where we should mention that for shared-memory machines it is necessary that each individual polynomial in the vector is stored separately from the others, i.e., they may not compete for memory space. The data structure for polynomials that we used assigned an array of memory space of fixed size to each polynomial wherein individual monomials could be allocated dynamically.

Having computed the traces on each node we collect them and compute their sum. This sum is stored and when we have run through all the cases we compute the complementary partition functions, that is, those with states $\sigma L$ having $\mu(L) > 0$. At this point we then have $Z^*$, $Z^{**}$ and $\overline{Z^*}$ from which we may (finally) obtain $Z$, see Eq. (2).

A word on memory requirements; as a rule of thumb the number of monomials needed to store each polynomial is a little less than $n^4/2$. Each monomial consists of a coefficient and two exponents. Observe that the coefficients requires slightly less than $n^2-n$ binary digits (since we keep $n$ vertices fixed). Let us say that the last $n$ bits are reserved for the exponents (this is rough counting). There are two vectors to be stored of size at most $2^{\lfloor n/2 \rfloor}$. The total memory used is then less than $n^6 2^{n/2}$ bits. The traditional method requires on the order of $n^6 2^n$ bits of memory.

## 5. PHYSICAL QUANTITIES

In this section we will define some physical quantities that can be extracted from the combinatorial partition function, see, e.g., refs. 10–12. In the next section we will analyse the data.

**Definition 5.1.** With $N = n^2$, the physical partition function is

$$Z_n(K, H) = Z(C_n \times C_n; e^K, e^H)$$

where $K = -J/k_B T$ and $H = -h/k_B T$ are the traditional parameters describing the interaction through the edges and an external magnetic field respectively. $T$ is the absolute temperature and $k_B$ is Boltzmann's constant. We will refer to $K$ as the coupling (or inverse temperature) and $H$ as the external field. The critical coupling is $K_c = \operatorname{arctanh}(\sqrt{2}-1) = \frac{1}{2}\log(\sqrt{2}+1) \approx 0.440687$.

We will also let $Z_n(K) = Z_n(K, 0)$ and write $Z$ instead of $Z_n$, $Z_n(K)$ or $Z_n(K, H)$ when the context is clear.

Henceforth we let $\tilde{v}$ denote relative energy, i.e., if the energy is $i$ then $\tilde{v} = i/m$ is the relative energy, where $m$ is the number of edges in the graph, so that $-1 \leqslant \tilde{v} \leqslant 1$. Analogously, we let $\tilde{\mu}$ denote the relative magnetisation, i.e., if the magnetisation is $j$ then $\tilde{\mu} = j/N$ is the relative magnetisation, so that $-1 \leqslant \tilde{\mu} \leqslant 1$.

As is traditional, see, e.g., ref. 12, we assume the Boltzmann distribution on the states and define

**Definition 5.2.** Given $K$ and $H$ the probability of being in the state $\sigma$, having energy $i$ and magnetisation $j$, is

$$\Pr[\sigma] = \frac{e^{iK+jH}}{Z}$$

Since the sum of the probabilities should be 1 we have

$$Z = \sum_{\sigma} e^{v_\sigma K + \mu_\sigma H}$$

Recalling Definition 2.3 of the coefficients $a_{i,j}$ the probability of being in any state with energy $i$ and magnetisation $j$ is then

$$\Pr[v = i, \mu = j] = \frac{a_{i,j} e^{iK+jH}}{Z}$$

Finally, the probability of being in any state with energy $i$ is

$$\Pr[v = i] = \sum_{j} \Pr[v = i, \mu = j] = \sum_{j} \frac{a_{i,j} e^{iK+jH}}{Z}$$

Thanks to this definition it is easy to obtain moments (about zero) of the magnetisation. Taking the $k$th derivative of $Z$, with respect to $H$, divided by $Z$ gives us

$$\begin{aligned}
\frac{Z^{(k)}}{Z} &= \frac{\sum_{i,j} j^k a_{i,j} e^{iK+jH}}{Z} = \sum_{i} \sum_{j} j^k \Pr[v = i, \mu = j] \\
&= \sum_{i} \sum_{j} j^k \Pr[\mu = j \mid v = i] \Pr[v = i] \\
&= \sum_{i} \mathrm{E}[\mu^k \mid v = i] \Pr[v = i] = \mathrm{E}[\mu^k]
\end{aligned}$$

and moments for relative magnetisation are of course obtained when dividing by $N^k$. Taking the first and second derivatives of $\log Z$ gives us the first and second moments

$$\frac{\partial \log Z}{\partial H} = \frac{Z'}{Z} = \mathrm{E}[\mu]$$

and

$$\frac{\partial^2 \log Z}{\partial H^2} = \frac{Z''}{Z} - \left(\frac{Z'}{Z}\right)^2 = \mathrm{E}[\mu^2] - \mathrm{E}[\mu]^2 = \mathrm{Var}[\mu]$$

Note by the way that all odd derivatives of $Z$ (with respect to $H$) are identically zero if $H = 0$, that is, $Z^{(k)}|_{H=0} \equiv 0$ if $k$ is odd. This is easily shown by the following:

$$\begin{aligned} Z^{(k)} &= \sum_{i,j} j^k a_{i,j} e^{iK+jH} = \sum_i e^{iK} \left( \sum_{j>0} j^k a_{i,j} e^{jH} + \sum_{j<0} j^k a_{i,j} e^{jH} \right) \\ &= \{a_{i,j} = a_{i,-j}\} = \sum_i e^{iK} \left( \sum_{j>0} j^k a_{i,j} e^{jH} - \sum_{j>0} j^k a_{i,j} e^{-jH} \right) \\ &= \sum_i e^{iK} \sum_{j>0} j^k a_{i,j} (e^{jH} - e^{-jH}) \end{aligned}$$

Setting $H = 0$ also makes every term zero. Without an external field the expected magnetisation is then always zero and the variance is the same as the second moment $\mathrm{E}[\mu^2]$.

Having evaluated $Z^{(k)}(K, 0)$ for odd $k$ we continue with the even $k$. Somewhat frustratingly we can only give explicit formulae for $K = H = 0$. On the other hand they are valid for all graphs. First we observe that it follows from the definition of the coefficients $a_{i,j}$ that

$$\sum_i a_{i,j} = \binom{N}{\frac{N-j}{2}}$$

Beginning with the simplest case, the 0th derivative, we have

$$Z(0, 0) = \sum_{i,j} a_{i,j} = 2^N$$

The second derivative (with respect to $H$) is

$$\begin{aligned} Z^{(2)}(0, 0) &= \sum_{i,j} j^2 a_{i,j} = \sum_j j^2 \sum_i a_{i,j} = \sum_j j^2 \binom{N}{\frac{N-j}{2}} \\ &= [\text{let } \ell = (N-j)/2] = \sum_\ell (N-2\ell)^2 \binom{N}{\ell} = N2^N \end{aligned}$$

where the last identity can be obtained from, e.g., Mathematica. Continuing in the same manner we get

$$Z^{(4)}(0,0) = (3N^2 - 2N)\, 2^N$$
$$Z^{(6)}(0,0) = (15N^3 - 30N^2 + 16N)\, 2^N$$
$$Z^{(8)}(0,0) = (105N^4 - 420N^3 + 588N^2 - 272N)\, 2^N$$

The $k$th derivative of $\log Z$ with respect to $H$ is called the $k$th order cumulant of the magnetisation and we will take a look at them when $H = 0$. Let $\mathscr{C}_k$ denote this quantity. Since each term of the odd derivatives contain odd derivatives of $Z$ (thus being zero) we are interested only in the cumulants of even order. The fourth order cumulant is

$$\mathscr{C}_4 = \left.\frac{\partial^4 \log Z}{\partial H^4}\right|_{H=0} = \frac{Z^{(4)}}{Z} - 3\left(\frac{Z''}{Z}\right)^2$$

which then is a function of $K$. What one actually studies is the cumulant ratio,

$$R_4 = 1 - \frac{Z^{(4)} Z}{3(Z'')^2} = 1 - \frac{Z^{(4)}/Z}{3(Z''/Z)^2}$$

which is the cumulant of the distribution normalised to mean 0 and variance 1. Since $\mathscr{C}_2 = Z''/Z$ and $Z^{(4)}/Z = \mathscr{C}_4 + 3\mathscr{C}_2^2$ we have that

$$R_4 = 1 - \frac{\mathscr{C}_4 + 3\mathscr{C}_2^2}{3\mathscr{C}_2^2} = \frac{-\mathscr{C}_4}{3\mathscr{C}_2^2}$$

The sixth order cumulant is

$$\mathscr{C}_6 = \frac{Z^{(6)}}{Z} - 15\frac{Z^{(4)} Z''}{Z^2} + 30\left(\frac{Z''}{Z}\right)^3$$

Then $Z^{(6)}/Z = \mathscr{C}_6 + 15\mathscr{C}_2\mathscr{C}_4 + 15\mathscr{C}_2^3$ and the ratio is

$$R_6 = 1 - \frac{Z^{(4)} Z}{2(Z'')^2} + \frac{Z^{(6)} Z^2}{30(Z'')^3} = \frac{\mathscr{C}_6}{30\mathscr{C}_2^3}$$

As an alternative way to produce higher derivatives of $\log Z$ we should mention that

$$\frac{1}{N}\log Z(0,H) = \log(2\cosh H) = \log 2 + \sum_{k=2}^{\infty} \frac{B_k\, 2^k\, (2^k - 1)\, H^k}{k!\, k}$$

where $B_k$ are the Bernoulli numbers ($B_k = 0$ for odd $k > 1$) defined by

$$\frac{t}{e^t - 1} = \sum_{k=0}^{\infty} B_k \frac{t^k}{k!}$$

What about derivatives with respect to $K$? Let us quickly repeat the above in that case. The first derivative then becomes $\mathrm{E}[v]$ and the second derivative gives us $\mathrm{Var}[v]$. A standard quantity used in statistical physics is the so called specific heat (a.k.a. heat capacity) and it is obtained from the next derivative with respect to $T$, i.e., the temperature.

$$\frac{\partial^2 \log Z}{\partial T\, \partial K} = \frac{\partial^2 \log Z}{\partial K^2} \frac{\partial K}{\partial T} = \frac{-k_B}{J} K^2 \mathrm{Var}[v]$$

**Definition 5.3.**

$$\text{Free energy} \quad \mathscr{F} = \frac{1}{N} \log Z,$$

$$\text{internal energy} \quad \mathscr{E} = \frac{\partial \mathscr{F}}{\partial K}, \qquad \text{specific heat} \quad \mathscr{H} = K^2 \frac{\partial \mathscr{E}}{\partial K},$$

$$\text{magnetisation} \quad \mathscr{M} = \frac{\partial \mathscr{F}}{\partial H}, \qquad \text{susceptibility} \quad \chi = \frac{\partial \mathscr{M}}{\partial H},$$

$$\text{fourth order cumulant ratio} \quad \mathscr{R}_4 = \frac{-\chi^{(2)}}{3N\chi^2},$$

$$\text{sixth order cumulant ratio} \quad \mathscr{R}_6 = \frac{\chi^{(4)}}{30N^2\chi^3}$$

where $\chi^{(k)}$ is the $k$th derivative of $\chi$ with respect to $H$. Also, for the cumulants it is assumed that $H = 0$.

Inserting the expressions for $Z(0, 0)$ we obtain the following values at $K = H = 0$

$$\mathscr{F} = \log 2, \qquad \chi = 1, \qquad \chi^{(2)} = -2, \qquad \chi^{(4)} = 16,$$

$$\mathscr{R}_4 = \frac{2}{3N} = \mathrm{o}(1), \qquad \mathscr{R}_6 = \frac{8}{15N^2} = \mathrm{o}(1)$$

When necessary we will index the quantities with the linear size of the graph. Note that the free energy is just a normalised form of $\log Z$. We

have used this normalisation so that the formulae will match the Onsager solutions below. With these definitions $\mathscr{E} = \mathrm{E}[v]/N$ so that $-m/N \leqslant \mathscr{E} \leqslant m/N$. For 2-dimensional square grids we then have $-2 \leqslant \mathscr{E} \leqslant 2$, for 3-dimensional cubic grids we have $-3 \leqslant \mathscr{E} \leqslant 3$ etc. Thus $N\mathscr{E}/m = \mathrm{E}[\tilde{v}]$. Also, $-1 \leqslant \mathscr{M} \leqslant 1$, that is, $\mathscr{M} = \mathrm{E}[\tilde{\mu}]$ and $\chi/N = \mathrm{Var}[\tilde{\mu}]$.

### 5.1. The Onsager Solutions

For completeness we state the Onsager solutions (with $J = -1$), see, e.g., refs. 13, 10–12, for the infinite 2-dimensional square grid which we will view as the limit curves of the quantities stated in the previous section when $n \to \infty$.

Let $\mathscr{K}_1$ be the complete elliptic integral of the first kind defined by

$$\mathscr{K}_1(x) = \int_0^{\pi/2} (1 - x \sin\theta)^{-1/2} \, \mathrm{d}\theta$$

Let $\mathscr{K}_2$ be the complete elliptic integral of the second kind defined by

$$\mathscr{K}_2(x) = \int_0^{\pi/2} (1 - x \sin\theta)^{1/2} \, \mathrm{d}\theta$$

Also let

$$k = \frac{2\sinh(2K)}{\cosh^2(2K)}$$

The free energy for the infinite grid is

$$\mathscr{F}_\infty(K) = \log 2 + \frac{1}{2\pi^2} \int_0^\pi \int_0^\pi \log[\cosh^2(2K) - \sinh(2K)(\cos u + \cos v)] \, \mathrm{d}u \, \mathrm{d}v$$

Note that

$$\mathscr{F}_\infty(K_c) = \frac{\log 2}{2} + \frac{2G}{\pi} \approx 0.929695$$

where $G \approx 0.915966$ is Catalan's constant. The internal energy for the infinite grid is

$$\mathscr{E}_\infty(K) = \coth(2K) \left( 1 + \frac{2}{\pi} \mathscr{K}_1(k^2)(2\tanh^2(2K) - 1) \right)$$

The specific heat for the infinite grid is

$$\mathscr{H}_\infty(K) = \frac{2}{\pi} K^2 \coth^2(2K) \left[ 2\mathscr{K}_1(k^2) - 2\mathscr{K}_2(k^2) - 2(1 - \tanh^2(2K)) \times \left( \frac{\pi}{2} + \mathscr{K}_1(k^2)(2\tanh^2(2K) - 1) \right) \right]$$

The spontaneous magnetisation $\mathscr{M}_s = \lim_{H \to 0^+} \lim_{n \to \infty} \mathscr{M}_n$ is given by

$$\tilde{\mu} = \mathscr{M}_s(K) = \begin{cases} (1 - \sinh^{-4}(2K))^{1/8} & K > K_c \\ 0 & K \leqslant K_c \end{cases}$$

This last formula was first formulated by Onsager in 1948 and derived by Yang in 1952. A full proof with references is found in ref. 11 (chapter 10). The inverse of the spontaneous magnetisation follows immediately,

$$K = \mathscr{M}_s^{-1}(\tilde{\mu}) = \frac{\operatorname{arcsinh}(1 - \tilde{\mu}^8)^{-1/4}}{2}$$

We will often need to convert between coupling $K$ and relative energy $\tilde{v}$ and for this purpose we use the Onsager solution for internal energy. In the special case of 2-dimensional square grids we then have $\tilde{v} = \mathscr{E}_\infty(K)/2$ and in the other direction, $K = \mathscr{E}_\infty^{-1}(2\tilde{v})$. We ignore the problem of actually formulating the inverse and use numerical methods instead. Using this formula in combination with the formula for the inverse of the spontaneous magnetisation we obtain

$$\tilde{v} = Q(\tilde{\mu}) = \frac{\mathscr{E}_\infty(\mathscr{M}_s^{-1}(\tilde{\mu}))}{2} \tag{3}$$

This gives us a formula describing the relation between the relative energy and relative magnetisation when $n \to \infty$.

The critical coupling $K_c$ is related to the critical relative energy through the formula $\tilde{v}_c = 1/2 \tanh(2K_c)$, and from this we obtain $\tilde{v}_c = 1/\sqrt{2} \approx 0.7071$.

We finish this subject by just mentioning that $Q(\tilde{\mu})$, plotted in Fig. 15, has a surprisingly good approximation through the much simpler formula

$$Q(\tilde{\mu}) \approx \frac{1}{\sqrt{2}} + \left(1 - \frac{1}{\sqrt{2}}\right) \tilde{\mu}^6 \tag{4}$$

which could be used in some practical circumstances. In fact, the difference between them is less than 0.00253.

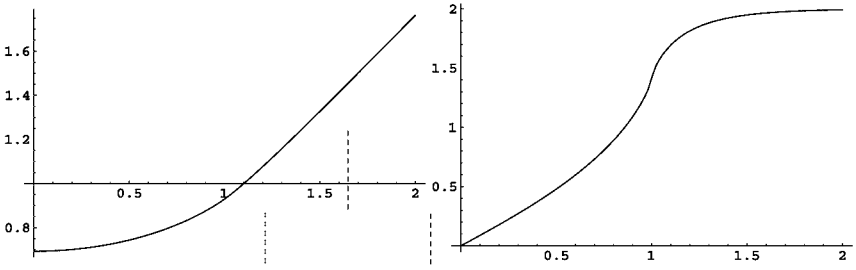


Fig. 5. Free energy $\mathscr{F}_\infty(K)$ and internal energy $\mathscr{E}_\infty(K)$ vs $K/K_c$.

Figure 5 show plots of $\mathscr{F}_\infty$ and $\mathscr{E}_\infty$. Had we added these plots for, say $n = 64$, they would hardly be distinguishable from the limit curves. In Fig. 6 we see $\mathscr{H}_n$ (for $n = 4, 8, 16, 32, 64, \infty$) and $\mathscr{M}_s$. We will return to the subject of $\mathscr{M}_s$ in a later section.

## 6. SCALING AT THE CRITICAL TEMPERATURE

We begin with a gallery of pictures. The left picture in Fig. 7 displays the magnetisation versus coupling and external field for the $14 \times 14$ grid. For an infinite grid we would have a jump in the magnetisation along the $H$-axis when $K > K_c$. The right picture shows the magnetisation at the critical coupling for a secuence of graphs.

Next, in Fig. 8 we look at the normalised susceptibility $\chi/N$ and the quotient $-\chi^{(2)}/\chi^{22/7}$ vs $K/K_c$ at $H = 0$ for $n = 3,\ldots, 15$.

Note that the plots of $-\chi^{(2)}/\chi^{22/7}$ has a local maximum before reaching the critical coupling $K_c$. For an infinite graph this maximum is supposed to be approximately 4.93, see ref. 5. The maxima clearly have a bit to go before reaching that value. The exponent $22/7$ is suggested by the theory of critical exponents. According to this, $\chi^{(2k)}(K) \propto (K_c - K)^{-\gamma - 2k\Delta}$ as $K \to K_c$ from below, see, e.g., ref. 14. Here $\gamma = 7/4$ is the susceptibility exponent

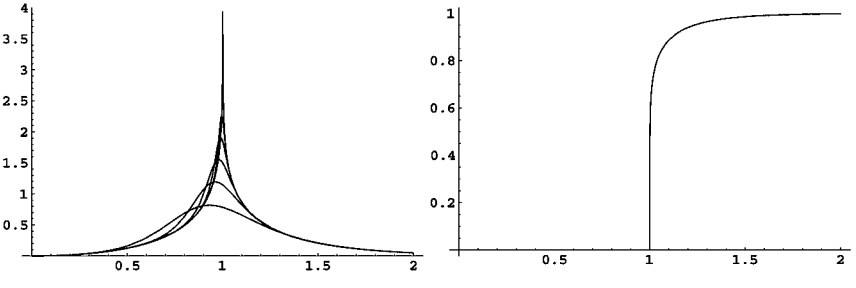


Fig. 6. Specific heat $\mathscr{H}_n(K)$ vs $K/K_c$ (for $n = 4, 8, 16, 32, 64, \infty$) and the spontaneous magnetisation $\mathscr{M}_s(K)$ vs $K/K_c$.

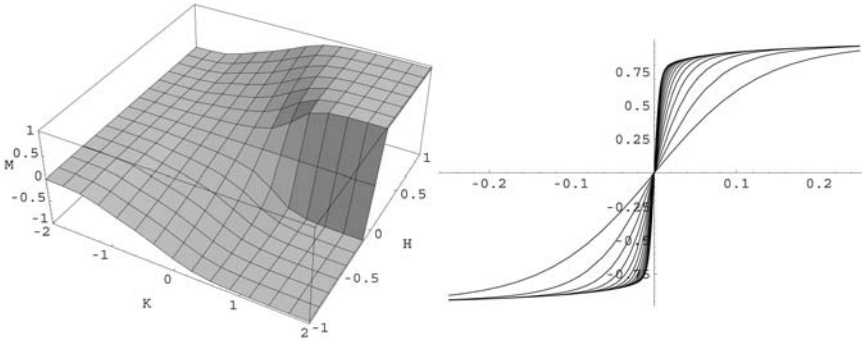


Fig. 7. Left: $\mathscr{M}_{14}$ vs $K/K_c$ and $H$. Right: $\mathscr{M}_n$ vs $H$ at $K_c$, $n = 3,\ldots, 15$.

and $\Delta = 15/8$ is the gap exponent. For $k = 1$ this gives the exponent $(\gamma + 2\Delta)/\gamma = 22/7$.

Figure 9 shows the fourth and sixth order cumulants $\mathscr{R}_4$ and $\mathscr{R}_6$ at $H = 0$. For large graphs the fourth and sixth cumulant goes to zero when $K \to 0^+$. Going in the other direction they behave as $\mathscr{R}_4 \to 2/3$ and $\mathscr{R}_6 \to 8/15$ when $K \to \infty$, see ref. 15.

Having stated and plotted the quantities of interest we shall take a closer look at their values at the critical coupling without an external field and see how they scale. In Table I we have tabulated the values of the various quantities and they match those stated by Baker.[5] Following his example we estimate an asymptotic value by using linear projections, i.e., plotting the values versus $1/n$, fitting a straight line to each pair of consecutive points and reading off the value at 0, see Table II. If we assume that the sequences in the last three columns of Tables I and II are strictly monotonous then we would have that the limiting value for $-\chi^{(2)}/\chi^{22/7}$ is in the interval (1.65333, 1.66133). Similarly, for $\mathscr{R}_4$ we would get the interval (0.610103, 0.611541) and for $\mathscr{R}_6$ the interval (0.463892, 0.465520).

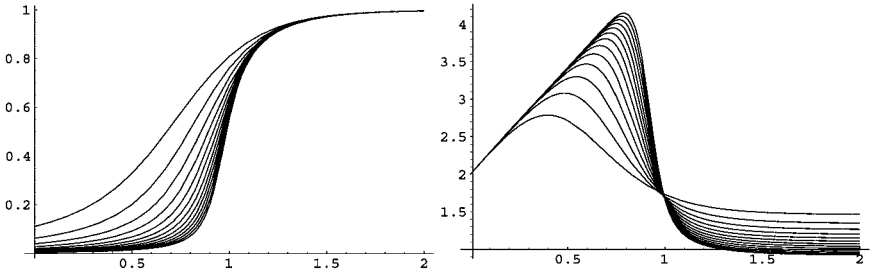

Fig. 8. $\chi/N$ (left) and $-\chi^{(2)}/\chi^{22/7}$ (right) vs $K/K_c$ at $H = 0$ for $n = 3,\ldots, 15$.

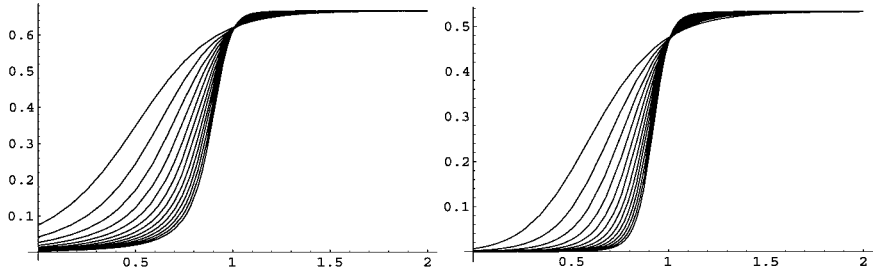


Fig. 9. Cumulants $\mathscr{R}_4$ (left) and $\mathscr{R}_6$ (right) vs $K/K_c$ at $H = 0$ for $n = 3,\ldots, 15$.

**Table I. Values at $K = K_c$ and $H = 0$**

| $n$ | $\chi$ | $-\chi^{(2)}$ | $\chi^{(4)}$ | $-\chi^{(2)}/\chi^{22/7}$ | $\mathscr{R}_4$ | $\mathscr{R}_6$ |
|---|---|---|---|---|---|---|
| 3 | 7.28487 | 888.591 | $4.46422 \times 10^5$ | 1.73075 | 0.620147 | 0.475197 |
| 4 | 12.1817 | 4396.28 | $6.55156 \times 10^6$ | 1.70159 | 0.617199 | 0.471905 |
| 5 | 18.0924 | 15110.1 | $5.21870 \times 10^7$ | 1.68707 | 0.615476 | 0.469970 |
| 6 | 24.9594 | 41334.5 | $2.83355 \times 10^8$ | 1.67882 | 0.614356 | 0.468707 |
| 7 | 32.7407 | 96687.6 | $1.18270 \times 10^9$ | 1.67366 | 0.613590 | 0.467841 |
| 8 | 41.4023 | 201764. | $4.07457 \times 10^9$ | 1.67019 | 0.613045 | 0.467224 |
| 9 | 50.9159 | 385941. | $1.21270 \times 10^{10}$ | 1.66773 | 0.612644 | 0.466770 |
| 10 | 61.2568 | 689322. | $3.21637 \times 10^{10}$ | 1.66591 | 0.612341 | 0.466426 |
| 11 | 72.4035 | $1.16480 \times 10^6$ | $7.77151 \times 10^{10}$ | 1.66453 | 0.612105 | 0.466159 |
| 12 | 84.3373 | $1.88025 \times 10^6$ | $1.73877 \times 10^{11}$ | 1.66346 | 0.611918 | 0.465947 |
| 13 | 97.0410 | $2.92082 \times 10^6$ | $3.64702 \times 10^{11}$ | 1.66260 | 0.611767 | 0.465776 |
| 14 | 110.500 | $4.39134 \times 10^6$ | $7.24039 \times 10^{11}$ | 1.66191 | 0.611643 | 0.465636 |
| 15 | 124.699 | $6.41882 \times 10^6$ | $1.37093 \times 10^{12}$ | 1.66133 | 0.611541 | 0.465520 |

**Table II. Linear Projections**

| Pair of $n$ | $-\chi^{(2)}/\chi^{22/7}$ | $\mathscr{R}_4$ | $\mathscr{R}_6$ |
|---|---|---|---|
| 3–4 | 1.61414 | 0.608358 | 0.462029 |
| 4–5 | 1.62897 | 0.608580 | 0.462228 |
| 5–6 | 1.63760 | 0.608760 | 0.462394 |
| 6–7 | 1.64268 | 0.608995 | 0.462645 |
| 7–8 | 1.64588 | 0.609230 | 0.462905 |
| 8–9 | 1.64804 | 0.609436 | 0.463136 |
| 9–10 | 1.64959 | 0.609607 | 0.463329 |
| 10–11 | 1.65074 | 0.609747 | 0.463488 |
| 11–12 | 1.65162 | 0.609862 | 0.463618 |
| 12–13 | 1.65231 | 0.609957 | 0.463726 |
| 13–14 | 1.65287 | 0.610037 | 0.463816 |
| 14–15 | 1.65333 | 0.610103 | 0.463892 |

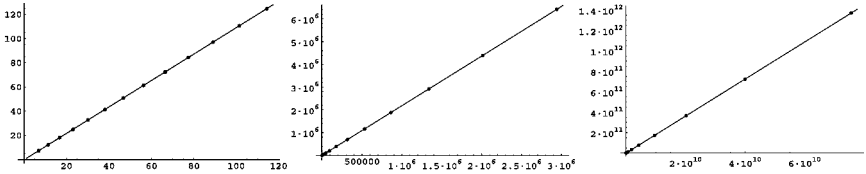

Fig. 10. $\chi$ vs $n^{7/4}$, $-\chi^{(2)}$ vs $n^{11/2}$ and $\chi^{(4)}$ vs $n^{37/4}$ at $K_c$.

Finite-size scaling theory predicts that $\chi(K_c) \sim n^{\gamma/\nu}$ where the correlation exponent $\nu = 1$ for 2D grids, see, e.g., ref. 16. Analogously to what we said above we then expect $\chi^{(2k)}(K_c) \sim n^{\gamma+2k\Delta}$. For $k = 1$ this gives the exponent $11/2$ and for $k = 2$ the exponent $37/4$. Plotting $\chi$ versus $n^{7/4}$ gives a more or less perfect fit to a straight line. The same holds for $-\chi^{(2)}$ versus $n^{11/2}$ and $\chi^{(4)}$ versus $n^{37/4}$, see Fig. 10. Calculating the slopes of the tangents through pairs of consecutive points in these figures gives us Table III, each column strictly monotonous. An estimate for the limiting value of $\chi^{(2)}/\chi^{22/7}$ at $K = K_c$ and $H = 0$ can now be obtained by using the numbers on the last line in Table III, namely $2.183160/1.092005^{22/7} \approx 1.6556$. For the fourth cumulant we get $2.183160/3/1.092005^2 \approx 0.61026$ and for the sixth cumulant $18.12481/30/1.092005^3 \approx 0.46396$. These estimates all end up inside the intervals mentioned above.

## 6.1. On the Negative Side: Anti-Ferromagnetic Curi(e)osities

As we have seen, our data on their own give us a fairly good idea about the behaviour of the susceptibility at the critical coupling. But what about the anti-ferromagnetic side? As one might expect the susceptibility

**Table III. Slopes of Consecutive Tangents**

| Pair of $n$ | $\chi$ | $\chi^{(2)}$ | $\chi^{(4)}$ |
|---|---|---|---|
| 3–4 | 1.094227 | 2.155778 | 17.70511 |
| 4–5 | 1.093600 | 2.168906 | 17.89712 |
| 5–6 | 1.092866 | 2.174581 | 17.98712 |
| 6–7 | 1.092465 | 2.177551 | 18.03531 |
| 7–8 | 1.092266 | 2.179341 | 18.06421 |
| 8–9 | 1.092163 | 2.180515 | 18.08301 |
| 9–10 | 1.092105 | 2.181330 | 18.09595 |
| 10–11 | 1.092068 | 2.181918 | 18.10525 |
| 11–12 | 1.092044 | 2.182356 | 18.11215 |
| 12–13 | 1.092027 | 2.182691 | 18.11742 |
| 13–14 | 1.092015 | 2.182952 | 18.12154 |
| 14–15 | 1.092005 | 2.183160 | 18.12481 |

**Table IV. Values at $-K_c$**

| $n$ | $\chi$ | $\chi^{(2)}$ | $\chi^{(4)}$ |
|---|---|---|---|
| 3 | 0.314282 | 0.0998332 | 0.581554 |
| 4 | 0.132012 | −0.450649 | 0.237996 |
| 5 | 0.245970 | −0.0803537 | 0.206457 |
| 6 | 0.141021 | −0.539504 | 0.589793 |
| 7 | 0.220060 | −0.176586 | −0.00995785 |
| 8 | 0.145477 | −0.603225 | 1.02357 |
| 9 | 0.206176 | −0.242816 | −0.133967 |
| 10 | 0.148149 | −0.652862 | 1.49646 |
| 11 | 0.197465 | −0.293701 | −0.2101 |
| 12 | 0.149931 | −0.693546 | 1.99224 |
| 13 | 0.191475 | −0.335126 | −0.257903 |
| 14 | 0.151205 | −0.728028 | 2.50327 |
| 15 | 0.187100 | −0.370097 | −0.287064 |

vanishes as $K \to -\infty$, but in the vicinity of $-K_c$ something peculiar is going on. The left plot of Fig. 11 shows the behaviour of $\chi$ around $-K_c$, the odd $n$ approaching from above, the even $n$ from below. Are they converging to the same limit curve? The values of $\chi(-K_c)$ plotted versus $1/n$ looks very much like a straight line. As we did at the end of the previous section we fit a straight line to the last two points, see the right plot of Fig. 11. For even $n$ this line intersects the y-axis at 0.158850 and for odd $n$ this happens at 0.158664. It is tempting to suggest that the limit is located inside this interval but, alas, it was shown in ref. 17 (we thank one of the referees for this reference) that the correct value is 0.15886652296 which falls just outside our interval. It is somewhat surprising though that we get four correct digits by studying such small grids.

A distinguishing feature of the anti-ferromagnetic side is the difference in behaviour between odd and even grids. On the ferromagnetic side there are no such discernible differences.

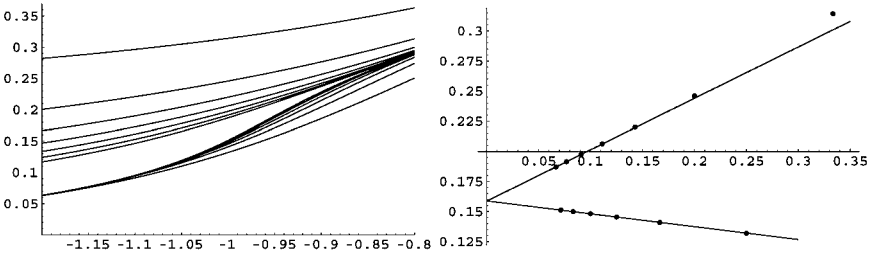


Fig. 11. Left: $\chi$ vs $K/K_c$. Right: $\chi$ at $K = -Kc$ vs $1/n$.

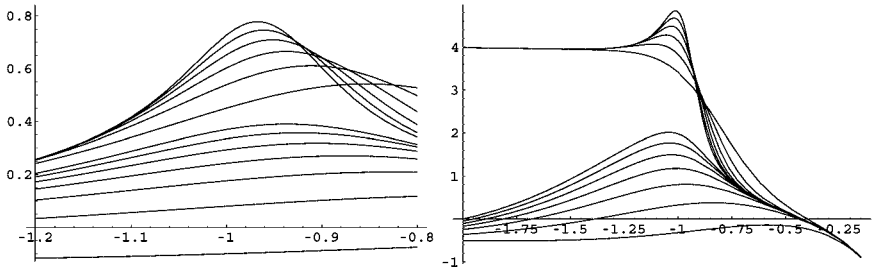


Fig. 12. $\chi^{(2)}$ (left) and $\chi^{(2)}/\chi$ (right) vs $K/K_c$

Figure 12 displays $\chi^2$ and $\chi^{(2)}/\chi$, in both cases the even $n$ are above the odd $n$. The behaviour is quite similar for higher derivatives as well.

The susceptibility and its derivatives vanishes as $K \to -\infty$ though they do so at different rates. The quotient between these rates are possibly constants. We finish this section by guessing some limits when $n \to \infty$ and $K \to -\infty$, in fact, the statements seems to hold for all fixed even $n$, though only for large odd $n$.

$$\chi^{(2)}/\chi \to -\tfrac{1}{2} \quad \text{for odd } n, \qquad \chi^{(2)}/\chi \to 4 \quad \text{for even } n$$
$$\chi^{(4)}/\chi \to 1 \quad \text{for odd } n, \qquad \chi^{(4)}/\chi \to 16 \quad \text{for even } n$$

## 7. THE POLYNOMIALS

Let us now take a look at the coefficients of the polynomials. We dismiss the empty energies and magnetisations though. We see here a phenomenon which is found in many graphs and in particular seems to be the rule for the square shaped grids, namely that above a certain critical energy the distribution of the magnetisations undergoes a phase transition; we go from a unimodal distribution to a bimodal distribution, giving the coefficients a horn-shaped feature, see the contour plot of Fig. 13 which is normalised so that at each energy the greatest coefficient is 1. An early study of this phenomenon can be found in ref. 15, see also ref. 18. There are more complicated phase transitions in our data; thus for instance oblong grids, say of the form $C_n \times C_{3n}$ appear to have a phase transition where the coefficients jump from a unimodal to a trimodal distribution before eventually settling down to a bimodal distribution. These facts shall be featured more prominently elsewhere. There is also a region close to the border where the distribution of coefficients on a nonempty energy level tend to have small local maxima in the interior, the left plot of Fig. 14 shows this phenomena. This phase transition shall not be discussed further.

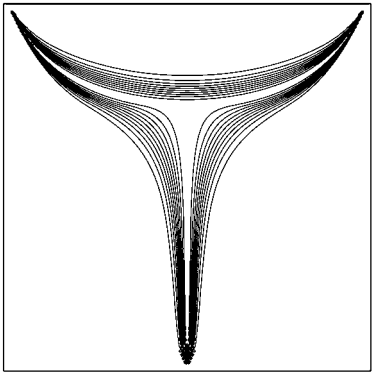

| $n$ | $\nu_c$ | $\tilde{\nu}_c$ |
|---|---|---|
| 3 | 2 | 0.1111 |
| 4 | 8 | 0.2500 |
| 5 | 10 | 0.2000 |
| 6 | 16 | 0.2222 |
| 7 | 30 | 0.3061 |
| 8 | 44 | 0.3438 |
| 9 | 58 | 0.3580 |
| 10 | 76 | 0.3800 |
| 11 | 98 | 0.4050 |
| 12 | 124 | 0.4306 |
| 13 | 150 | 0.4438 |
| 14 | 180 | 0.4592 |
| 15 | 214 | 0.4756 |

Fig. 13. Left: Coefficients for $14 \times 14$. Normalised to max coefficient 1 at each energy. Magnetisation on the x-axis and energy on the y-axis. Right: Table of critical energies.

The right plot of Fig. 14 displays the local maxima along the energies. This curve looks suspiciously like a perfect $x^2$ curve and indeed that is what it is. Actually, given a fixed magnetisation $j$, the expected energy of an edge $e = \{u, v\}$, and thus the expected relative energy, can be determined exactly. This is done in ref. 18 from which we quote the following formulae. Let us denote by $k$ the number of $+1$ spins, i.e., $k = (N+j)/2$. Then the number of states with $\sigma_u = \sigma_v = +1$ is $\binom{N-2}{k-2}$, the number of states with both spins $-1$ is $\binom{N-2}{k}$ and the number of states with different spins is $2\binom{N-2}{k-1}$. In total, the expected energy on edge $e$ is

$$\begin{aligned}
\mathrm{E}[\tilde{\nu} \mid \mu = j] = \mathrm{E}[\sigma_u \sigma_v \mid \mu = j] &= \frac{\binom{N-2}{k-2} - 2\binom{N-2}{k-1} + \binom{N-2}{k}}{\binom{N}{k}} \\
&= \frac{N^2 - N - 4Nk + 4k^2}{N^2 - N} = [\text{with } k = (N+j)/2] \\
&= 1 - \frac{N^2}{N^2 - N} + \frac{j^2}{N^2 - N} \sim \left(\frac{j}{N}\right)^2 = \tilde{\mu}^2
\end{aligned}$$

Higher moments can be determined as well, but we will leave this matter after just saying that the distribution (i.e., of energies) is highly concentrated around its mean.

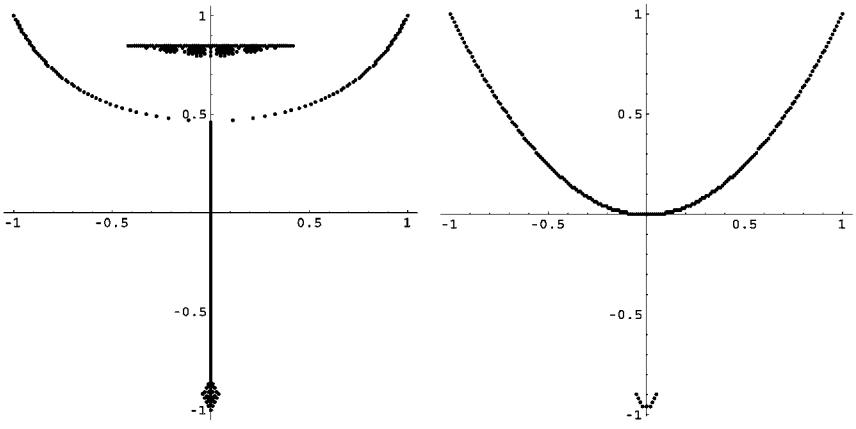


Fig. 14. Locations of local maxima for $n = 14$ along the magnetisations (left) and energies (right). Magnetisation on the x-axis and energy on the y-axis.

If we focus our attention on the unimodal to bimodal phase transition (the existence of which by the way does not seem to be established rigorously), the question is then, at what critical energy does this take place and what is the asymptotic behaviour for our given family of graphs?

**Definition 7.1.** The critical energy $v_c$ of a graph $G$ is the maximum energy where the distribution of magnetisations is unimodal.

The table in Fig. 13 lists where this phase transition takes place for our graphs. In the next section we will return to this subject. The left plot of Fig. 15 shows how the distributions of the magnetisations (i.e., the sum is normalised to 1) change for the $14 \times 14$ grid as the energy increases, from unimodal to bimodal. Binder[15] plots similar curves based upon sampled data (versus temperature though).

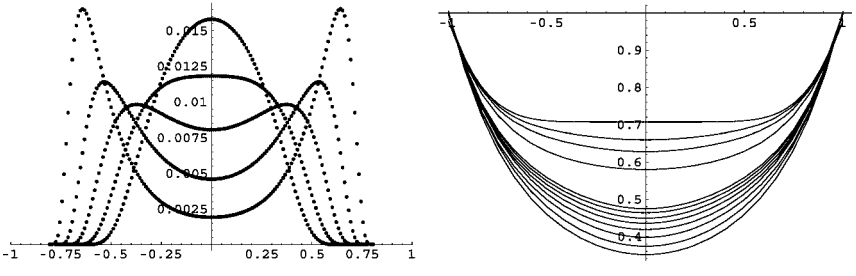


Fig. 15. Left: distributions for $n = 14$ at energies 160, 180, 200, 220 and 240. Right: location of peaks vs $\tilde{\mu}$ for $n = 8,\ldots, 15, 32, 64, 128, \infty$.

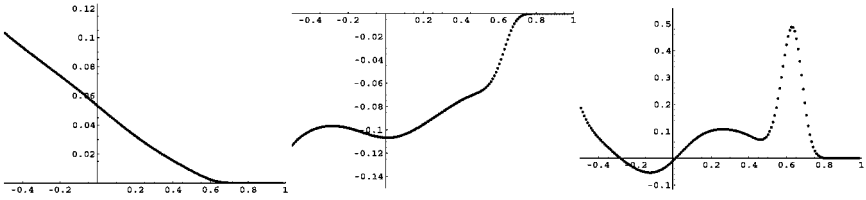

Fig. 16. The sequence $a_{i,1}/a_i$ vs $i/m$ and its first and second derivatives for $n = 15$.

The right plot of Fig. 15 shows the locations of the peaks of the distributions for all the exactly computed graphs. It also shows the peaks for the $32 \times 32$, $64 \times 64$ and the $128 \times 128$ grid, based on sampled data, and the asymptotic peak obtained from Eq. (3) above. We will return to this in the next subsection.

From the left plot of Fig. 15 we see that the probability for zero-magnetisation goes to zero as the energy increases. In Fig. 16 we plot the quotient $a_{i,1}/a_i$ versus $i/m$ for the $15 \times 15$ grid (i.e., the middle-magnetisation; for even grids one should plot $a_{i,0}/a_i$) together with its first and second derivatives.

## 7.1. The Shape of the Horn

Due to the Onsager formula for spontaneous magnetisation we know what the relative magnetisation will be at each coupling (for a large graph), and $\tilde{\nu} = Q(\tilde{\mu})$ in Eq. (3) expresses the inverse returning the relative energy instead. We have not yet defined this for finite graphs however. For a finite graph we define the peak magnetisation at a given energy as the location of the peak in the distribution of the magnetisation.

**Definition 7.2.** Let the sequence of $a_{i,j}$ be given and let $A_i = \max_j a_{i,j}$. At energy $i$ the peak magnetisation $P_n(i/m)$ is the greatest $j/N$ such that $A_i = a_{i,j}$. We also define $Q_n(j/N) = P_n^{-1}(|j/N|)$ and set $Q_n(0) = \tilde{\nu}_c$.

Thus $Q_n$ describes the shape of the horn of Fig. 13 in terms of relative magnetisation. We will tacitly assume that the peak magnetisation approaches the spontaneous magnetisation as $n \to \infty$. It should be possible to prove that the distribution actually becomes concentrated in this manner as $n$ grows, though we will not attempt this here. The right plot in Fig. 15 shows $Q_n(\tilde{\mu})$ for $n = 8, \ldots, 15, 32, 64, 128, \infty$ (after interpolation) and this plot clearly suggests that $Q_n \to Q$ as $n \to \infty$. The natural question at this point is to ask what the difference between the limiting $Q$ and the individual $Q_n$ is and at what rate the difference vanish with increasing $n$.

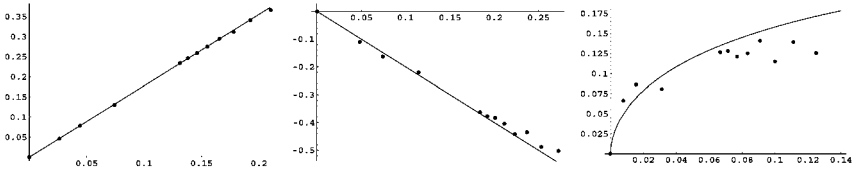

Fig. 17. 0th, 2nd and 4th coefficient vs $n^{-3/4}$, $n^{-5/8}$ and $n^{-1}$ resp. for $n = 8,\ldots, 15, 32, 64, 128, \infty$.

The difference $Q - Q_n$ seems to be nicely fit by a 4th degree polynomial so we will settle for this. In Fig. 17 we plot, from left to right, the coefficients of $x^0$ versus $n^{-3/4}$, the coefficients of $x^2$ versus $n^{-5/8}$ and the coefficients of $x^4$ versus $n^{-1}$ respectively. Together with the data points are also shown the guessed functions $16x/9$, $-2x$ and $2x^{5/8} - 16x^{3/4}/9$ respectively. This last function determines itself since we want the function to go through the points $(\pm 1, 0)$. The plots are based upon data for $n = 8,\ldots, 15, 32, 64, 128, \infty$ (we use sampled data for $n = 32, 64, 128$).

First, and most important, the 0th coefficient says at what energy the distribution of magnetisations goes from unimodal to bimodal. The straight line fitted here is rather convincing. The coefficient $16/9 \approx 1.777$ is a nice square but we might as well suggest the more elegant $\sqrt{\pi} \approx 1.772$.

For the 2nd coefficient the straight line is perhaps less convincing, determining the correct exponent of $n$ is not that easy in this case. Somewhat disappointing, as the last picture shows, the fit is not very good for the 4th coefficient. However, this does not seem to matter all that much since the suggested approximation function in Eq. (5) gives a virtually perfect fit to the real data.

$$Q_n(x) \approx Q(x) - [\tfrac{16}{9} n^{-3/4} - 2n^{-5/8} x^2 - (\tfrac{16}{9} n^{-3/4} - 2n^{-5/8})\, x^4] \qquad (5)$$

## 7.2. The Variance of the Horn

If we look at one side of the distributions shown in Fig. 15 we see how their widths vary with increasing energy. It seems that around the critical energy, just before the distribution becomes bimodal, the width is at its greatest. Let us then look at how the variance of the relative magnetisation changes with the relative energy. However, we only look at the variance of the absolute magnetisations, i.e., $\mathrm{Var}[|\tilde{\mu}|]$.

The first plot in Fig. 18 shows this variance for $n = 8,\ldots, 15, 32, 64$ and 128 (again, 32, 64, 128 are based upon sampled and slightly smoothed data). In the limit when $n \to \infty$ we expect the variance to approach zero,

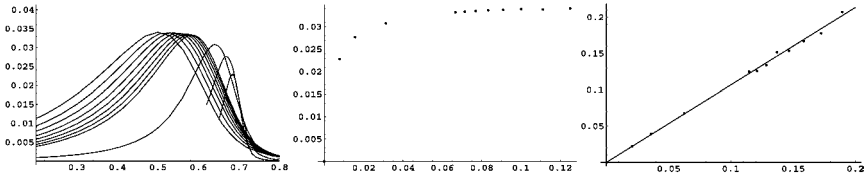

Fig. 18. Left: Var$[|\tilde{\mu}|]$ vs $\tilde{\nu}$ for $n = 8,\ldots, 15, 32, 64, 128$. Middle: maxVar$[|\tilde{\mu}|]$ vs $n^{-1}$. Right: $\frac{1}{\sqrt{2}}-$maxloc Var$[|\tilde{\mu}|]$ vs $n^{-4/5}$.

i.e., all the magnetisations concentrate on the shape of spontaneous magnetisation and are zero below $1/\sqrt{2}$. The plots in Fig. 18 supports this claim.

The maximum variance tends to decrease as $n$ grows, but at what rate? The second plot in Fig. 18 shows the maximum variance versus $1/n$ but we have no good suggestion of what formula these points obey. That the variance is slowly decreasing should be clear though.

Where is the maximum variance located? As $n \to \infty$ we expect it to approach $1/\sqrt{2}$. The last plot of Fig 18 shows the difference between the location of the maximums and $1/\sqrt{2}$ versus $n^{-4/5}$ together with the guessed function $16x/15$. The fit is quite convincing, so we dare suggest that the location of the maximum is in the vicintity of $1/\sqrt{2}-\frac{16}{15}n^{-4/5}$.

## REFERENCES


1. B. A. Cipra, An introduction to the Ising model, *Amer. Math. Monthly* **94**:937–959 (1987).
2. P. Beale, Exact distribution of energies in the two-dimensional Ising model, *Phys. Rev.* **76**:78–81 (1996).
3. P. H. Lundow, Compression of transfer matrices. Technical Report 5 (Department of Mathematics, Umeå University, 1999).
4. P. H. Lundow, Computation of the Ising partition function for grid graphs. Technical Report 14 (Department of Mathematics, Umeå University, 1999).
5. G. A. Baker, The Markov property method applied to Ising model calculations, *J. Stat. Phys.* **77**:955–976 (1994).
6. N. Biggs, *Interaction Models* (Cambridge University Press, 1977).
7. D. Babic *et al.*, The matching polynomial of a polygraph, *Discrete Appl. Math.* **15**:11–24 (1986).
8. P. H. Lundow, Multiprecision integers: A Fortan 90 module. Manuscript, 2000.
9. P. H. Lundow, Polynomials: A Fortran 90 module. Manuscript, 2000.
10. C. J. Thompson, *Mathematical Statistical Mechanics* (Princeton University Press, 1972).
11. B. M. McCoy and T. T. Wu, *The Two-Dimensional Ising Model* (Harvard University Press, 1973).
12. D. A. Lavis and G. M. Bell, *Statistical Mechanics of Lattice Systems* (Springer, 1999).
13. L. Onsager, Crystal statistics I. A two-dimensional model with an order-disorder transition. *Phys. Rev. (2)* **65**:117–149 (1944).
14. C. Domb, Ising Model, in *Phase Transitions and Critical Phenomena*, Vol. 3, C. Domb and M. S. Green, eds. (Academic Press, 1972).

15. K. Binder, Finite size scaling analysis of Ising model block distribution functions, *Z. Phys. B-condensed matter* **43**:119–140 (1981).
16. M. N. Barber, Finite-size scaling, in *Phase Transitions and Critical Phenomena*, Vol. 8, C. Domb and J. L. Lebowitz, eds. (Academic Press, 1983).
17. X. P. Kong, H. Au-Yang, and H. H. Perk, Logarithmic Singularities of Q-dependent susceptibility, *Phys. Letts. A*, **118**:336–340 (1986).
18. R. Häggkvist and A. Rosengren, Some conjectures concerning the coefficients in the Ising polynomial. Manuscript, 1997.